

Approved.  
Nadeem Hashem  
  
23/06/2014

Revised version approved  
Ridwan Ben Hamada  
  
  
Sunith Pathirana.

QATAR UNIVERSITY  
Graduate Studies  
College of Arts and Sciences

**AN INTEGRATED APPROACH TO BENTHIC HABITAT  
CLASSIFICATION OF THE NORTH EASTERN QATAR  
MARINE ZONE USING REMOTE SENSING,  
GEOGRAPHIC INFORMATION SYSTEM, AND IN SITU  
MEASUREMENTS**

A Technical Report in  
Environmental Sciences

By

© 2014 Sanaa Arif Hobeichi

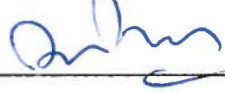
Submitted in Partial Fulfillment  
of the Requirements  
for the Degree of  
Master of Science

June 2014

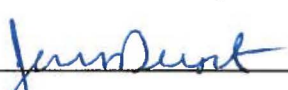
The thesis of **Sanaa Arif Hobeichi** was reviewed and approved by the following:

We, the committee members listed below accept and approve the Technical report of the student named above. To the best of this committee's knowledge, the technical report confirms the requirements of Qatar University, and we endorse this Technical report for examination.

Name **Dr. Sumith Pathirana**

Signature  Date 31/05/2014

Name **Dr. Jennifer Dupont**

Signature  Date 31/5/14

Name **Dr. Radhouan Ben Hamadou**

Signature  Date 31.5.2014

Name **Dr. Nadeem Hashem**

Signature  Date 31.05.2014

## **Abstract**

A key aspect in the conservation management of the coastal marine zone is mapping the benthic habitat, which is the focus of the work presented in this project. Multispectral Worldview-2 (WV2) satellite data acquired in April 2010 was used to classify and map the benthic habitat of the North-Eastern part of Qatar marine zone: A 35 km stretch of coastline, 7 km wide, with water depth ranging from 0 to 11 m. Baseline field surveys of the area of study carried out in March-April 2010 identified 4 broad benthic types: Seagrass, Algae, live corals and sand. WV2 data was corrected for atmospheric and water column effects. Depth-invariant bottom indices were calculated and formed the basis for classification. Field survey data was used to implement the supervised classification and accuracy assessment. From the result of the classification, an overall accuracy of 81.8% was obtained. The gap in the available information on the benthic cover in the Qatari coastal marine zone makes the study useful to detect changes in the benthic cover over time.

**Keyword:** Benthic cover Mapping, Benthic habitat, Remote sensing, Worldview-2, ENVI, Satellite Image processing, Water column correction, Qatar

## Table of Contents

Table of Contents.....	iv
List of Figures.....	viii
List of tables.....	x
List of abbreviations.....	xii
Acknowledgment.....	xiii
Dedication.....	xiv
Chapter 1.....	1
INTRODUCTION.....	1
1.1 Problem definition.....	1
1.2 Aims and Objectives.....	2
Chapter 2.....	3
BACKGROUND AND LITTERATURE REVIEW.....	3
2.1 Remote sensing process for benthic cover.....	3
2.2 WorldView-2 (WV2) satellite.....	3
2.2.1 WorldView-2 spectral bands.....	4
2.3 Image pre-processing.....	5
2.3.1 Radiometric Calibration.....	5
2.3.1.1 Relative Radiometric Calibration:.....	6
2.3.1.2 Absolute Radiometric Calibration:.....	6

2.3.1.2.1 Atmospheric correction:.....	7
2.3.1.2.1.1 The empirical line method.....	7
2.3.1.2.1.2 Second Simulation of a Satellite Signal in the Solar Spectrum (6S) method .....	8
2.3.1.2.1.3 Fast Line-of-sight Atmospheric Analysis of Hypercubes (FLAASH).....	8
2.3.2 Water column correction: .....	8
2.3.2.1 Lyzenga model.....	9
2.3.2.2 Bierwirth model .....	10
2.4 Image Classification.....	10
2.4.1 Unsupervised Classification .....	10
2.4.1.1 K-means .....	10
2.4.1.2 Iso-Data.....	11
2.4.2 Supervised classification .....	12
2.4.2.1 Maximum Likelihood Classification (MLC).....	12
2.4.2.2 Minimum Distance Classification (MDC).....	12
Chapter 3.....	13
METHODOLOGY AND PROCESSING .....	13
3.1 Study Area.....	13
3.1.2 Field Data .....	13

3.1.2.1 Benthic Habitats.....	14
3.1.3 Imagery.....	15
3.2 ENVI Image Processing Software .....	16
3.3 Image Processing Overview.....	17
3.3.1 Image Pre-processing .....	18
3.3.1.1 Masking .....	18
3.3.1.2 Radiometric Calibration.....	19
3.3.1.2.1 FLAASH atmospheric correction .....	19
3.3.1.3 Mosaicking.....	20
3.3.1.4 Resampling .....	21
3.3.1.5 Water Column Correction.....	21
3.3.1.6 Image Filtering.....	24
3.3.2 Image processing .....	24
3.3.2.1 Supervised Classification.....	25
3.3.2.2 Validation and Accuracy Assessment.....	26
Chapter 4.....	29
IMPLEMENTATION AND RESULTS.....	29
4.1 Water column correction.....	29
4.2 Supervised Classification .....	29
4.3 Accuracy Assessment.....	30

Chapter 5.....	32
DISCUSSION AND LIMITATION.....	32
5.1 Water Column Correction algorithm .....	32
5.2 Field data.....	32
5.3 Classification and accuracy assessment .....	33
Chapter 6.....	35
CONCLUSION.....	35
LIST OF REFERENCES.....	36
Annex A: Algorithm written in IDL to generate the depth-invariant index using Lyzenga method.....	40
Annex B : Maps showing benthic cover classification.....	42

## List of Figures

Figure 1 The effect of the water column and the atmosphere on the amount of radiance reaching the sensor over a water mass. (borrowed from Edward (1999); own elaboration) .....	4
Figure 2 : Reflectance of a benthic cover (Seagrass) measured at variant depth [17].....	9
Figure 3 : Schematic representation of K-means algorithm [19].....	11
Figure 4 : Distribution of the stations along the marine zone of the study area .....	14
Figure 5 : Type and percentage of benthic cover identified at each station .....	15
Figure 6 : WorldView-2 satellite images of the area of study delivered from DigitalGlobe as adjacent/overlapping tiles .....	16
Figure 7 : The flowchart of the general methodology applied in this project .....	17
Figure 8 : Masking the land area from a tile .....	18
Figure 9 : WorldView-2 image (at the left) delivered by DigitalGlobe with relative radiometric correction undergoes absolute radiometric correction and FLAASH atmospheric correction by applying two utilities in ENVI .....	20
Figure 10 : Twelve tiles of atmospherically corrected image (at the left) assembled in a single composite image (at the right) after applying seamless mosaic .....	20
Figure 11 : Graphical representation of the linearization of the depth/radiance relationship for a homogenous bottom type: Sand [24] [17] .....	21
Figure 12 : The regression line of the bi-plot ( $X_i$ against $X_j$ ) for a homogenous bottom type: Sand. The slope of the regression line represents the attenuation coefficient between the pair of bands $i$ and $j$ [24] [17] .....	22

Figure 13 : Different bottom types have the same attenuation coefficient (slope of the regression line) but a different depth invariant index ( $y - intercept$  of the regression line) for the same pair of bands  $i$  and  $j$  [24] [17] ..... 23

Figure 14 : Schematic representation of pixels classified using Maximum Likelihood Classification [19]..... 26

Figure 15 : Atmospherically corrected image in RGB (1), results of the final depth invariant index image for one band ratio: Red edge - Blue (2), Green-Yellow (3), Green-Infra red2 (4), Blue-Green (5) ..... 29

Figure 16 : Classification Results of MLC applied on 4 pre-processed images with different band ratios: Red edge – Blue (1), Green-yellow (2), Green-Infra red2 (3), Blue-Green (4) ..... 30

## **List of tables**

Table 1 : WorldView-2 traditional and new bands, band wavelengths (nm) and usefulness of each spectral band .....	5
Table 2 Metadata of the satellite imagery .....	15
Table 3 : Overall accuracy of the classification results after processing 4 index images .....	31
Table 4 : Confusion matrix calculated for the classification results of the index image with band ratio (green-yellow) .....	31
Table 5 : Producer and user accuracies and errors of commission and omission calculated for the classification results of the index image with band ratio (Green-Yellow) .....	31



## **List of abbreviations**

<b>BIL</b>	<b>Band Interleaved by Line</b>
<b>BPP</b>	<b>Bits Per Pixel</b>
<b>BSQ</b>	<b>Band Sequential</b>
<b>CSV</b>	<b>Comma Separated Values</b>
<b>DN</b>	<b>Digital Number</b>
<b>DII</b>	<b>Depth Invariant Index</b>
<b>DOC</b>	<b>Dissolved organic compounds</b>
<b>ENVI</b>	<b>Environment for Visualizing Images</b>
<b>EQ</b>	<b>Equation</b>
<b>EMR</b>	<b>Electromagnetic Radiation</b>
<b>ESC</b>	<b>Environmental Studies Center</b>
<b>FLAASH</b>	<b>Fast Line-of-sight Atmospheric Analysis of Hypercubes</b>
<b>GIS</b>	<b>Geographic Information System</b>
<b>GSD</b>	<b>Ground Sample Distance</b>
<b>IDL</b>	<b>Interactive Data Language</b>
<b>MODTRAN</b>	<b>MODerate resolution TRANsmission mode</b>
<b>MLC</b>	<b>Maximum Likelihood Classification</b>
<b>RGB</b>	<b>Red – Green - Blue</b>
<b>ROI</b>	<b>Region Of Interest</b>
<b>TOA</b>	<b>Top Of Atmosphere</b>
<b>WV2</b>	<b>World View-2</b>
<b>6S</b>	<b>Second Simulation of the Satellite Signal in the Solar Spectrum</b>

## **Acknowledgment**

I want to thank all the people that gave me the opportunity to do this project; Dr. Samir Jaoua, Dr. Nabil Al Zouari, Dr. Andrew Wigton and Dr. Eric Febbo

My sincere thanks to my supervisor Dr. Sumith Pathirana for his support and advice and for guiding me through the daily struggles. This project meant a lot of new knowledge and skills.

I also gratefully acknowledge Dr. Jennifer Dupont for supervising me at ExxonMobil, and for giving me constructive feedback and valuable ideas.

I also thank committee members Dr. Radhouan Bin Hamadou and Dr. Nadeem Hashem for their support.

Big thanks go to Aysegul Basar, for discussing relevant and irrelevant topics in her office at ExxonMobil.

Last but not least, I could not have worked on this project without the help of my husband and mom.

This work was supported by ExxonMobil Research Qatar and the Environmental Studies Center at Qatar University.

## **Dedication**

This work is dedicated to ExxonMobil Research Qatar.

## **Chapter 1**

### **INTRODUCTION**

#### **1.1 Problem definition**

Qatar National vision aims to achieve a sustainable development that ensures the balance between human development, economic development and the natural environment, where neither of which should be sacrificed for the sake of the other [1].

Human development on the coasts involves dredging and land reclamation for expanding residential areas, industries, and other projects. These all have a great impact on the coastal areas and adjacent marine habitats.

Habitat classification of benthic cover provides a tool to facilitate efficient assessment of the state of the benthic habitat, detect changes to the habitat, and to potentially mitigate the impacts of human development on benthic habitats and communities.

Characterization and classification of benthic habitat relies on field survey data which provides information on scattered areas of the benthic cover. In addition to the field data, the use of high resolution satellite image and advanced image processing techniques can generate continuous data of the benthic cover.

Benthic cover data captured via satellites and validated using field survey data provides a cost effective tool for benthic cover classification in accessible and inaccessible areas. Moreover Geographic Information System (GIS) can be used to store and manipulate benthic cover data and produce maps that show benthic cover classification.

Mapping and monitoring the benthic habitat of an undisturbed area is needed for a better protection of the benthic habitat and for preservation of their related ecosystem.

The area of study -North-Eastern part of Qatar- has been selected among all the other undisturbed areas due to the availability of data, which includes a set of satellite imagery (WorldView-2) and ground truth data. The study area is a 235 km<sup>2</sup> strip section of the North-Eastern Qatari coastline. This area is relatively undisturbed by human activities compared to the rest of the Eastern coastline that includes the major industrial cities in Qatar.

### **1.2 Aims and Objectives**

The aim of this project is to classify, map and validate the benthic habitat at the North-Eastern part of Qatar marine zone (QMZ), by combining remote sensing techniques, Geographic Information System (GIS) and field data.

In order to achieve this aim, the following specific objectives were considered:

- 1) Correct remotely sensed data by applying pre-processing techniques
- 2) Apply image processing techniques to corrected satellite data to identify and produce benthic habitat classification.
- 3) Validate the benthic habitat classification using field data
- 4) Produce maps of benthic habitat.

## **Chapter 2**

### **BACKGROUND AND LITTERATURE REVIEW**

#### **2.1 Remote sensing process for benthic cover**

The incident solar radiation received by the benthic cover is influenced by the absorption and scattering of the atmospheric components and the water column components. Optical satellites have sensors that are sensitive to the reflected and emitted electromagnetic radiation from the benthic cover and other features on the earth. Radiation passes through two media, the atmosphere and the water, and then back to the sensor (Figure 1). The radiation received by an optical remote sensor from the benthic cover is the result of the biotic/abiotic nature of the benthic environment combined with the influence of both the atmospheric and water column components.

Every substrate on the surface of the earth is characterized by its spectral reflectance signature which is the amount of the reflected electromagnetic radiation [2]. Different substances can be distinguished from each other by their spectral characteristics. Hence, it is possible to distinguish different types of benthic cover using satellite imagery, when proper correction techniques are applied and the data is validated using in situ (ground truth) data [3].

#### **2.2 WorldView-2 (WV2) satellite**

Worldview-2 satellite was launched by DigitalGlobe in October 2009. It orbits the earth in a sun synchronous orbit at an orbital altitude of 770 km. WV2 has an orbit period of about 100 minutes. On average, it can revisit any point on the globe every 1.1 days and able to capture about 1 million km<sup>2</sup> of area per day. WV2 has passive sensors that can detect the reflected energy when the source of energy is sun only. Therefore it cannot

be used at night because sun is not illuminating the earth at that time, unlike the active sensors that provide their own energy source for illumination by emitting radiation toward a target object, and then capture the radiation reflected from that target [4]. WV2 has a high spectral resolution sensor with 8-multispectral bands and one panchromatic band (Table1). WV2 has a high spatial resolution of 1.8 m in the multispectral mode and 46 cm in the panchromatic mode, with a dynamic range of 11 bits per pixel [5].

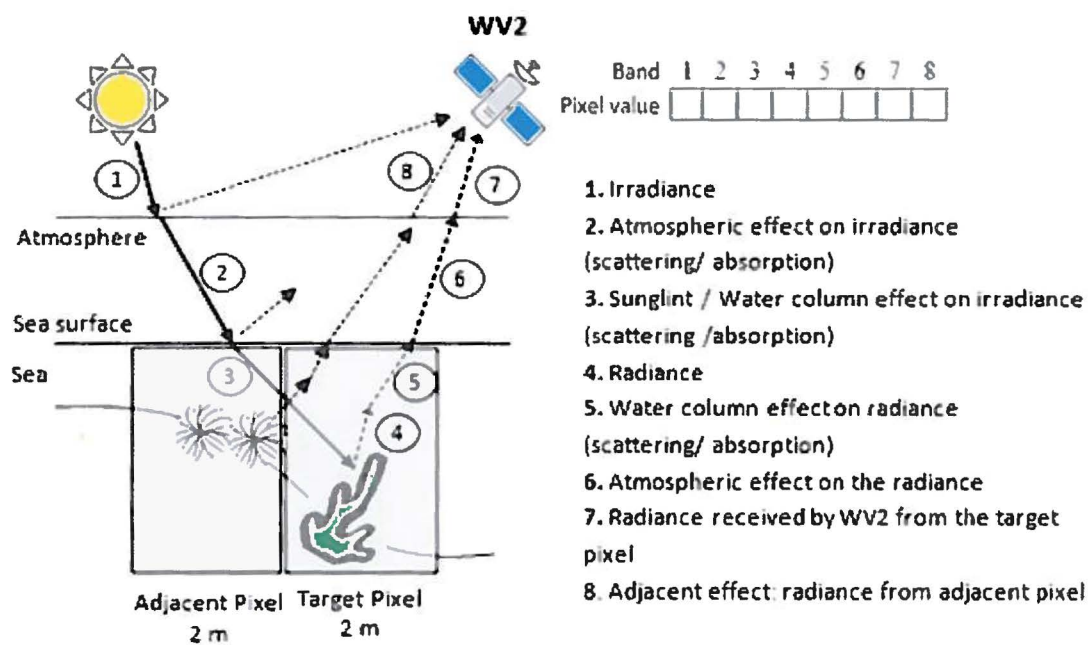


Figure 1 The effect of the water column and the atmosphere on the amount of radiance reaching the sensor over a water mass. (borrowed from Edward (1999); own elaboration)

### 2.2.1 WorldView-2 spectral bands

WV2 provides a high resolution panchromatic band (450 – 800 nm) and eight spectral bands that range from visible to near-infrared (400 – 1040 nm); the eight spectral bands include four traditional bands, and four new additional bands (Table1). WV2 spectral bands are designed to improve the segmentation and classification of

atmospheric, terrestrial and water features. The table below gives an overview of the role of each spectral band [5].

Table 1 : WorldView-2 traditional and new bands, band wavelengths (nm) and usefulness of each spectral band

	Traditional Bands	New Bands	Band Edge (nm)	usefulness	
WV2 Spectral Bands		Coastal blue	[ 400 – 450 ]	Vegetative analysis Bathymetric studies Improves atmospheric correction techniques	
		Blue	[ 442 – 515 ]	Detecting regions of water	
		Green	[ 510 – 580 ]	Vegetation analysis	
		Yellow	[ 585 – 625 ]	Feature classification Detects the “yellowness of particular vegetation, on land and in water	
		Red	[ 630 – 690 ]	Vegetation analysis	
			Red Edge	[ 705 – 745 ]	Measuring plant health Vegetation analysis
		Near Infrared 1 (NIR1)		[ 770 – 895 ]	Estimation of moisture content and plant biomass Classification of vegetation types Classification of soil types
			Near Infrared 2 (NIR2)	[ 860 – 1040 ]	Broad vegetation analysis Biomass studies

### 2.3 Image pre-processing

In benthic remote sensing, environmental conditions at the time when the image was taken and the characteristics of the water column have an effect on the intensity of the object’s radiance received by the sensor. Therefore, in order to obtain a relatively accurate spectral response of the object of interest, the satellite imagery should be pre-processed, and the effect of these components should be removed [3].

The main techniques for the pre-processing steps are presented below:

#### 2.3.1 Radiometric Calibration

Radiometric calibration is classified into two types; absolute and relative calibration. Relative radiometric calibration accounts for sensor characteristics, whereas absolute calibration accounts for illumination geometry and atmospheric effects.

### 2.3.1.1 Relative Radiometric Calibration:

Digital numbers recorded by a satellite must undergo a relative radiometric correction.

In fact, many deficiencies in the imagery can occur due to variability in detector response, variability in electronic gain and offset, lens falloff, and particulate contamination on the focal plane [6]. These deficiencies can be shown in the form of streaks and banding in imagery.

Normally, WV2 products are delivered with relative radiometric correction performed on raw data from all detectors in all bands. Relative radiometric correction minimizes image artifacts [7]. A further radiometric calibration step is required: Absolute radiometric calibration to account for earth-sun distance and azimuth angle.

### 2.3.1.2 Absolute Radiometric Calibration:

From each spot on the Earth's surface, optical satellites sensors detect the intensity of the electromagnetic radiation (EMR) as a digital number (DN), called also pixel value.

The DN of each image is specific to the type of sensor and is affected by the illumination geometry and the atmospheric condition during the image acquisition [8]. The conversion of DNs to reflectance values is required in order to obtain reliable information from satellite images [9], this process is called absolute radiometric calibration of images. Absolute radiometric calibration puts the data on a standard scale and makes it compatible with the data acquired from different sensors [10] and hence comparable with the data available in the spectral libraries.

The Absolute calibration is a two-step process:

1) The conversion of DN values to Top of atmosphere (TOA) spectral radiance:

TOA spectral radiance is the spectral radiance incoming towards the satellite at satellite's altitude [11].

2) The TOA spectral radiance is then converted into surface reflectance. This conversion involves the application of atmospheric correction methods on the TOA radiance values. The surface reflectance values provide a standardized measure which makes the comparison between images meaningful even if the images were taken by different sensors as well as in different time of the day, season or latitude [8].

#### *2.3.1.2.1 Atmospheric correction:*

The reflectance of the objects recorded by satellite sensors is generally affected by atmospheric absorption and scattering. These normally result in alteration of the actual reflectance of the objects that subsequently affects the extraction of information from images [12]. In order to make a meaningful measure of reflectance at the Earth's surface, the atmospheric interferences (absorption and scattering) must be removed from the data. This process is called "atmospheric correction" [8]. EMR interacts with gas molecules in the atmosphere such as greenhouse gases which reduce its intensity. This is called absorption. EMR interacts with airborne particulate matter (aerosols) and results in a redirection of the incident EMR and hence deflection of the reflected EMR from its path [8]. This phenomenon is called scattering. Atmospheric correction compensates for both atmospheric absorption and scattering [12].

#### **2.3.1.2.1.1 The empirical line method**

The empirical line method can be applied on multispectral satellite imagery to convert TOA spectral radiance to surface reflectance [13]. This method establishes a

relationship (linear or quadratic) between the TOA spectral radiance and the radiance values measured from calibration targets located within the image area. A prediction equation is then defined and used to convert the TOA radiance to surface reflectance for each band [14].

#### **2.3.1.2.1.2 Second Simulation of a Satellite Signal in the Solar Spectrum (6S)**

##### **method**

This method is highly effective for atmospheric correction for turbid coastal environments and shallow waters compared to other atmospheric correction methods. 6S is an algorithm designed to simulate the reflection of solar radiation by a coupled atmosphere-surface system for a wide range of atmospheric correction. In order to run 6S model, the meteorological visibility data should be available [12].

#### **2.3.1.2.1.3 Fast Line-of-sight Atmospheric Analysis of Hypercubes (FLAASH)**

FLAASH is another method for atmospheric correction. It is a first-principles atmospheric correction tool that operates in the spectral range (400 – 2500 *nm*). FLAASH provides basic atmospheric correction with the additional option of corrections for light scattered from adjacent pixels [15].

#### **2.3.2 Water column correction:**

EMR that penetrates water attenuates exponentially when the depth increases. The degree of attenuation of EMR is mainly due to two processes, absorption and scattering [16]. Absorption occurs when the electromagnetic energy is converted into other forms such as chemical energy or heat. Water, Algae, suspended particulate matter and Dissolved Organic Compounds (DOC) are highly absorbents of the red part of the

spectrum, but have a small effect on the blue part of the spectrum [2]. Scattering occurs when EMR interacts with suspended particles in the water column and changes direction. Therefore scattering increases in turbid water [3]. The spectra of the same stratum changes with depth (Figure 2). Similarly, the spectral signature of one substrate at one depth could be very similar to the spectra of another stratum at a different depth. Therefore, for benthic habitat classification and mapping it is important to remove the influence of water depth, scattering and absorption [2].

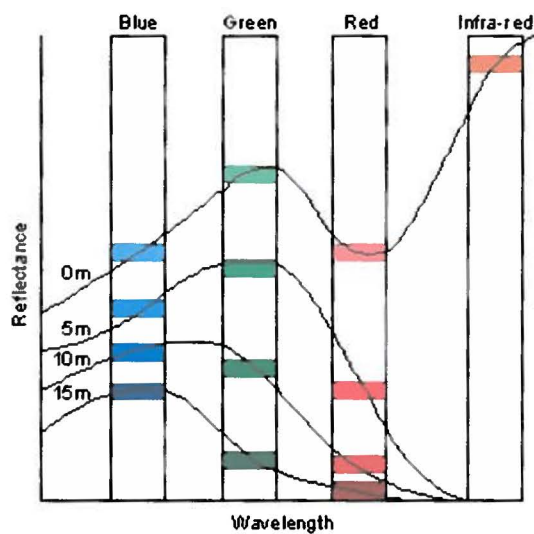


Figure 2 : Reflectance of a benthic cover (Seagrass) measured at variant depth [17]

### 2.3.2.1 Lyzenga model

Many studies related to benthic habitats mapping using remote sensing have adopted Lyzenga technique to minimize the effect of the water column [2] [18]. Lyzenga technique is used to calculate the ratios of attenuation coefficient for two bands and to produce a Depth Invariant Index (DII) of the bottom type by considering the water surface radiance for the used wavelength band pairs. This method is used to distinguish different bottom types. It assumes that the radiance ratios of two distinct benthic types are independent of water depth as long as the attenuation coefficients are the same in

each couple of bands. This method works truly in clear water or where the level of turbidity is invariant. DII can then be used for benthic cover classification [2].

#### 2.3.2.2 Bierwirth model

Bierwirth model is another model that can be implemented for water column correction [16]. This model computes the sea bottom reflectance based on the assumption that the attenuation coefficient is homogenous across the entire image and it requires the depth value for every pixel.

### 2.4 Image Classification

After the pre-processing steps, classification techniques can be applied on the corrected image to perform benthic habitat classification. There are two main types of classification: unsupervised classification and supervised classification.

#### 2.4.1 Unsupervised Classification

Unsupervised classification produces clusters of pixels based on the statistical analyses of spectral similarity of pixels. Pixels having similar spectral characteristics are grouped together in a distinct cluster. The two most common algorithms for unsupervised classification are K-means and ISO-Data.

##### 2.4.1.1 K-means

K-means classifier follows the following algorithm [19] (Figure 3):

1. Class centers of a number of *a priori* classes are positioned randomly through the space of pixels that are being clustered.
2. Pixels distances from the class centers are calculated and each pixel is assigned

to the class with the minimum distance.

3. The mean of the class is re-calculated taking into account all the pixels in the class.
4. Steps 2 and 3 are repeated until one of three conditions is met:
  - The centers of the classes are moving by a distance below predefined threshold.
  - The specified number of iterations reached its maximum
  - The percentage of moving pixels is below a predefined threshold.

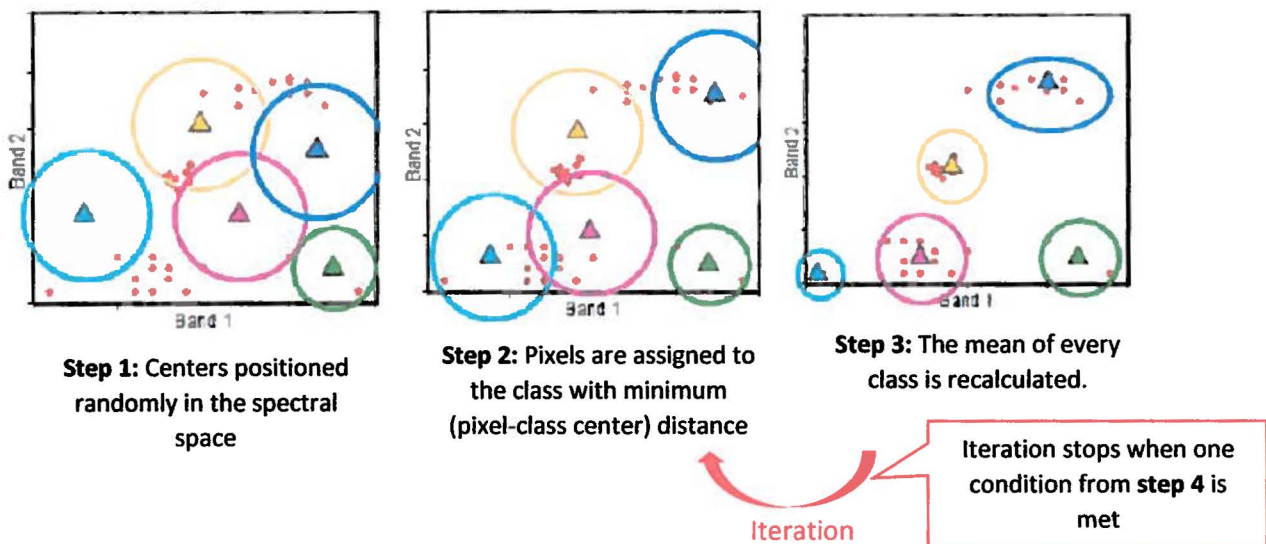


Figure 3 : Schematic representation of K-means algorithm [19]

#### 2.4.1.2 Iso-Data

Iso-Data algorithm works similarly to k-means algorithm with a few differences:

- The number of clusters is not fixed and the classes are subject to be split or merged.

- More input parameters are required. They are mainly predefined conditions to stop the iteration.

## **2.4.2 Supervised classification**

Supervised classification allocates pixels in a dataset to classes based on pre-defined training data. Predefined training data can be spectral signatures representing the various benthic cover types or Regions Of Interests (ROIs) that represent known benthic cover classes. The classifier assigns every pixel in the image to a particular benthic type as identified during the training process. Among the few available supervised classification techniques, Maximum Likelihood Classification (MLC) and Minimum Distance Classification (MDC) are the most adopted techniques.

### **2.4.2.1 Maximum Likelihood Classification (MLC)**

MLC is a widely used supervised classification method for benthic cover classification. It operates based on two principles [22]:

- It assumes that the statistics for each training class in each band are normally distributed
- It is based on the Bayesian probability theory (probability density function).

### **2.4.2.2 Minimum Distance Classification (MDC)**

MDC calculates the mean vectors for every class and evaluates the Euclidean distance from each image pixel to the mean vector of every class. First the mean vector for each category is determined from the average pixel value in each band for each class. An unknown pixel can then be classified by computing the distance from its spectral position to each of the means and assigning it to the class with the closest mean. One limitation of this technique is that it overlooks the different degrees of variation [22]

## **Chapter 3**

### **METHODOLOGY AND PROCESSING**

#### **3.1 Study Area**

The study area is a strip section of the North-Eastern Qatari coastline, stretching from the North of Ras Laffan to the South of Al Rewais. This is approximately a 35 km stretch of coastline, and the total area covers 235 km<sup>2</sup> with water depth ranging from 0 to 11 meters.

The study area is relatively undisturbed by human activities compared to the rest of the eastern coastline that includes major industrial cities. The project incorporates Field Data and Remotely Sensed Data.

##### **3.1.2 Field Data**

This project uses field data from the Ecological Baseline survey carried out by the Environmental Studies Center (ESC) of Qatar University in conjunction with ExxonMobil Research Qatar (EMRQ).

The study area was divided into 10 transects from the south to the north, running from land to the sea and spaced at 3.5 km interval along the shoreline. The survey includes a total of 44 stations: Along each transect, 4 stations were surveyed at 250, 1000, 2500 and 5000 meters from the shoreline. An additional station at 7000 meters was surveyed along 4 transects, where the width of the marine area is more than 5 km (Figure 4).

The field data incorporates data on the benthic cover. Scuba video surveys were carried out for a period of two months (from March to April 2010) along 100m transects. These surveys have been performed by a professional cameraman scuba diver, and a marine

biologist. Detailed analysis of the video-transects was further conducted at the ESC by a marine biologist and a GIS specialist on benthic community mapping. The field data was subsequently imported into GIS software to locate the benthic cover identified at each station (Figures 4 and 5).

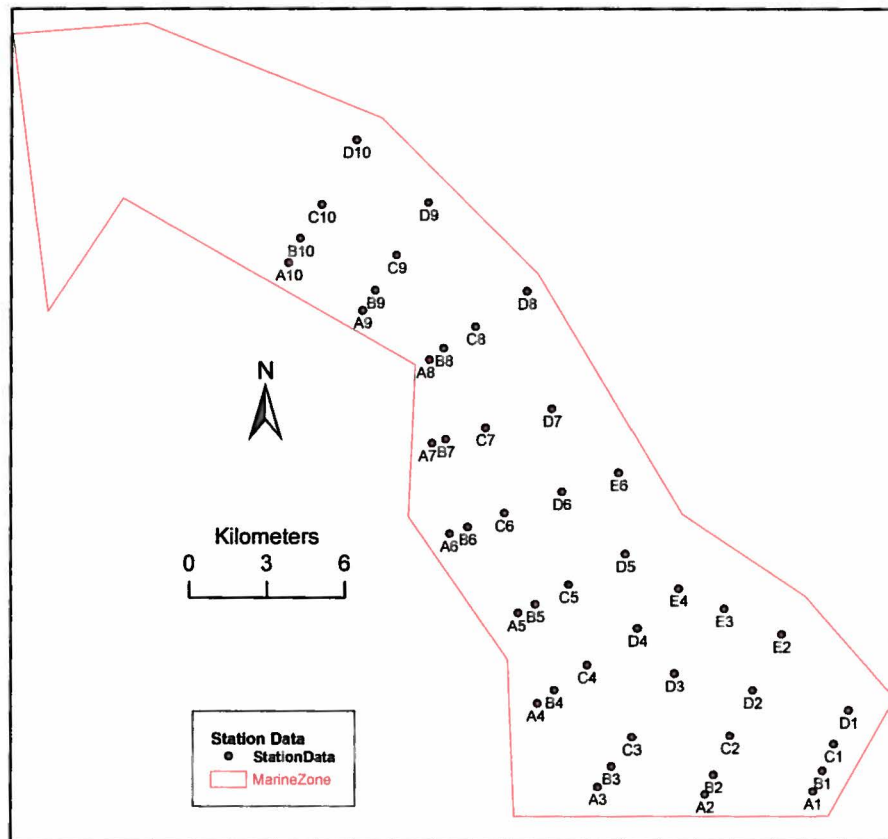


Figure 4 : Distribution of the stations along the marine zone of the study area

### 3.1.2.1 Benthic Habitats

Three broad types of benthic habitats have been detected on the videos:

- Seagrass: includes Seagrass meadows and seaweeds
- Coral: represented by live coral
- Algae: includes Macroalgae bed, the most encountered Macroalgae are brown

In the areas where there is no biological cover, the bottom type is sand or sand mixed with dead coral.

The percentage of each benthic cover type encountered on the videos was assigned according to the following classification.

0-5%	5-25%	25-50%	50-75%	75-100%
------	-------	--------	--------	---------

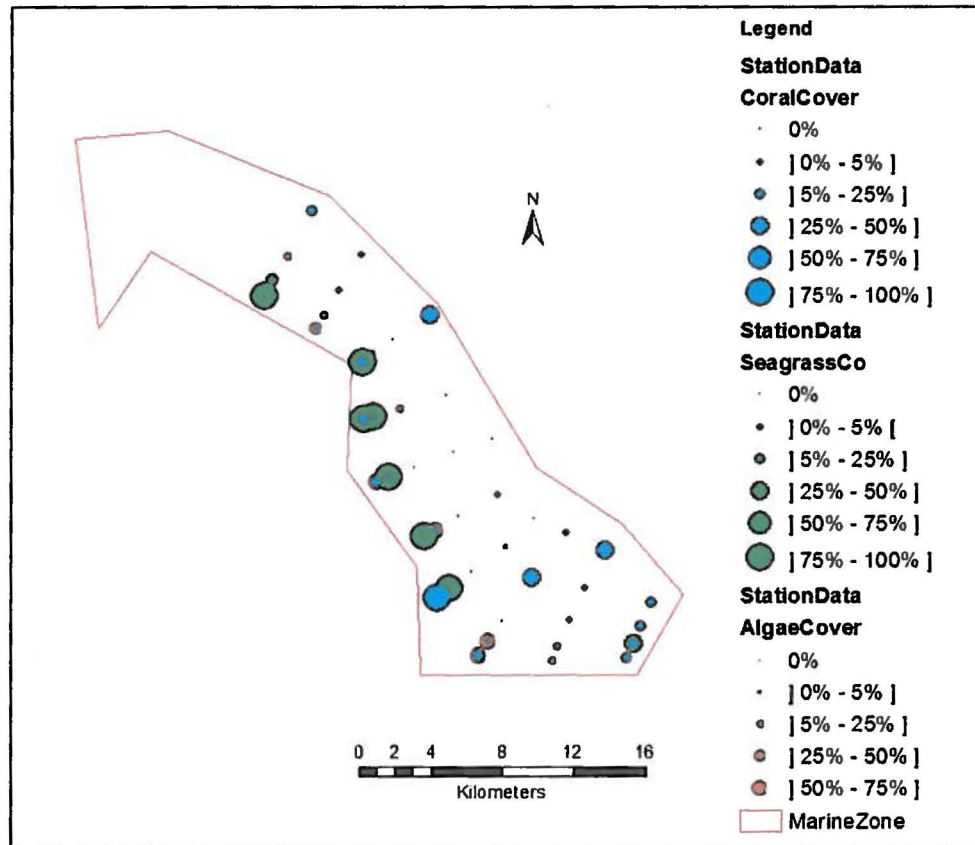


Figure 5 : Type and percentage of benthic cover identified at each station

### 3.1.3 Imagery

WV2 Multispectral images were available for the study area. The metadata of the images as delivered is shown in Table 2. The image data set covering the study area contained 12 WV2 images (tiles) (Figure 6) with pixel resolution of  $2m \times 2m$ .

Images with smaller sizes allow software packages such as ENVI, IDL and ArcMap to import and process the images [25].

Table 2 Metadata of the satellite imagery

Acquisition Date	Acquisition Time	Sun Elevation	Sun Azimuth	Cloud Cover
26/4/2010	7:21:35	69.4°	123.5°	0%

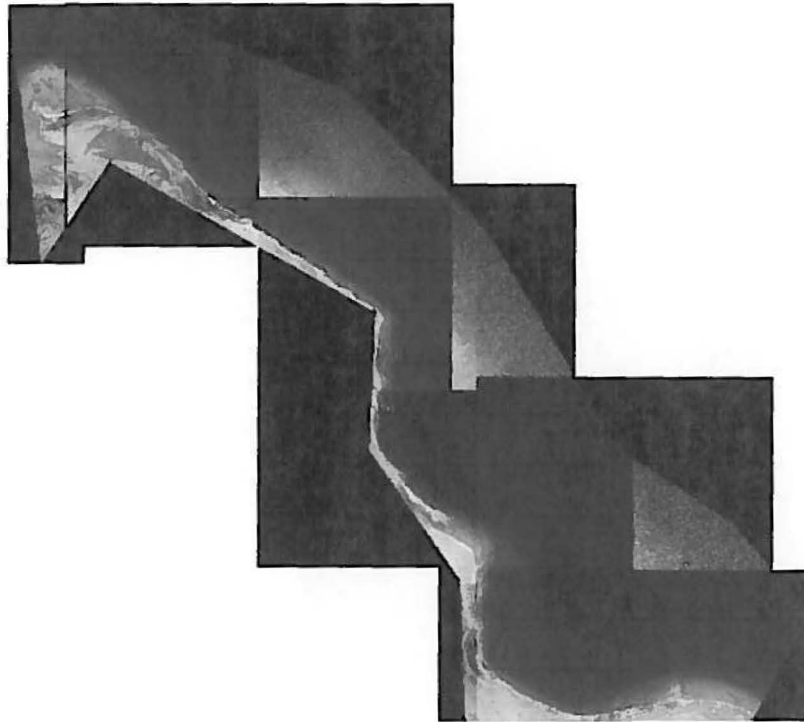


*Figure 6 : WorldView-2 satellite images of the area of study delivered from DigitalGlobe as adjacent/overlapping tiles*

### **3.2 ENVI Image Processing Software**

The satellite data was processed using ENVI (5.1) software. ENVI (ENvironment for Visualizing Images) is a software designed to process and analyze satellite imagery. ENVI package includes a number of scientific algorithms for image processing.

IDL (Interactive Data Language), is a programming language that can be used in ENVI environment to develop functions and procedures for pre-processing and processing satellite imagery. The ENVI Platform fully integrates with ArcMap, which increases the efficiency of image processing and data validation.

### 3.3 Image Processing Overview

The flowchart of the general methodology applied in this project is shown in Figure 7.

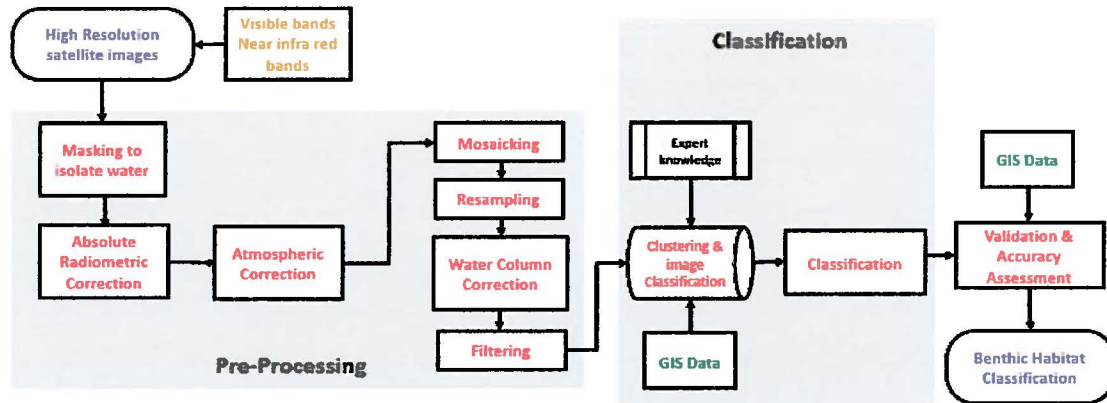


Figure 7 : The flowchart of the general methodology applied in this project

The first step involved acquiring the WV2 multispectral satellite imagery for the area of study. The land area was masked out from all the tiles to improve the contrast in digital numbers (DNs) for non-land areas. Then absolute radiometric calibration and correction were performed on the raw imagery and resulted in converting raw DN to top of atmosphere (TOA) spectral radiance. FLAASH atmospheric correction was then applied to convert TOA spectral radiance to surface spectral reflectance. Seamless mosaicking was applied to bind the tiles of reflectance images in one single image representing the area of study. The image was resampled to reduce its size and allow further processing. Eight spectral subsets were then created from the filtered reflectance image. Each subset displays the image in one band.

In order to remove the effect of the water column, a script for Lyzenga's water column correction model was written in IDL and executed on a 48 different pairs of spectral subsets and generated 48 depth-invariant-index images. Previous researches and visual interpretation were used to identify the band combinations of the spectral subsets that are appropriate to extract benthic cover features. The resultant images were filtered

using Bit errors filtering technique in ENVI (5.1) to remove the salt and pepper appearance. The field data showing the benthic cover (type and percentage of coverage) identified at 44 stations was stored in Excel (.csv) format and imported into ArcMap as GIS layers. The 44-station data points were randomly divided into two sets for classification and accuracy assessment: Accordingly, 22 data points were used as training data for implementing Maximum Likelihood Classification (MLC) and the remaining data points were used for accuracy assessment and for calculation of confusion matrix. And finally, maps of benthic cover classification: Seagrass, Macroalgae, coral and sand cover, were produced.

### 3.3.1 Image Pre-processing

WV2 images are typically delivered relatively radiometric-calibrated and the intensity of the electromagnetic radiation is recorded as DN's. The land area was masked out then absolute radiometric calibration and FLAASH atmospheric correction were applied.

#### 3.3.1.1 Masking

Polygons were drawn to cover the land area in the original WV2 images. Pixels covered by the polygons were masked out to exclude them from the image processing. Masking was applied on all the tiles that contain land surface. This was done by using two features in ENVI 5.1: "Masking" and "Region of interest" (ROI) (Figure 8).

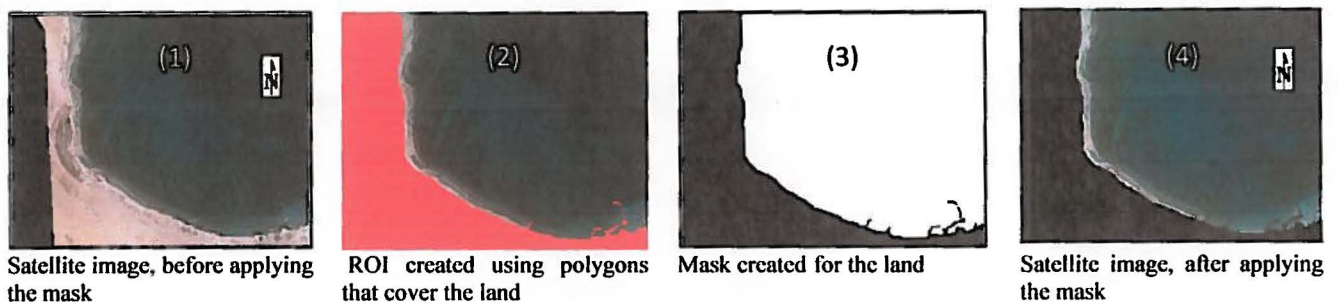


Figure 8 : Masking the land area from a tile

### 3.3.1.2 Radiometric Calibration

ENVI 5.1 has a specific absolute radiometric calibration utility for WV2 images. This utility was used to produce TOA radiance images in units of  $\frac{\mu W}{cm^2 \times sr \times nm}$ . This utility uses information in the metadata file of the image provided by DigitalGlobe and applies Gains and Offsets method. The equation used is this conversion is:

$$L_{sat} = DN \times Gain + Offset \quad (EQ 1)$$

Where  $L_{sat}$  is the spectral radiance that enters the satellite,  $DN$  is the digital number recorded by the sensor and  $Gain$  and  $Offset$  are calibration parameters specific to the sensor [20].

In this step, the image format was converted from Band Sequential (BSQ) to Band Interleaved by Line (BIL) format, to create a radiance image with required settings for input into FLAASH atmospheric correction module (Figure 8).

#### 3.3.1.2.1 FLAASH atmospheric correction

FLAASH atmospheric correction module was applied to remove the effects of the atmosphere and to convert the TOA radiance images into surface reflectance images (Figure 9). The calibrated radiance images were used as input and the scene characteristics were retrieved from the metadata file and entered in FLAASH Atmospheric Correction Model. The Tropical atmospheric model and the Urban aerosol model were selected for image analysis using FLAASH.

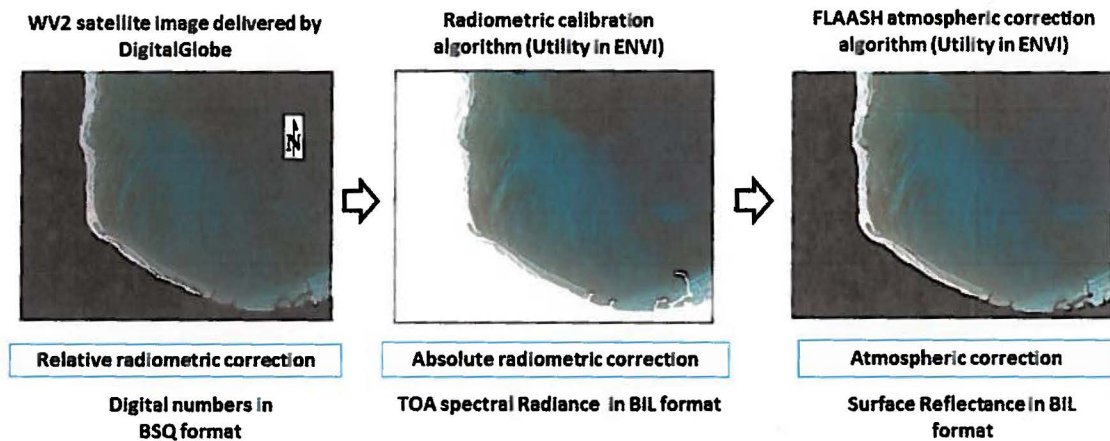


Figure 9 : WorldView-2 image (at the left) delivered by DigitalGlobe with relative radiometric correction undergoes absolute radiometric correction and FLAASH atmospheric correction by applying two utilities in ENVI

### 3.3.1.3 Mosaicking

Seamless Mosaic tool in ENVI 5.1 was used to assemble the 12 tiles of images into one single composite image that covers the area of study (Figure 10). While applying the mosaic tool, color correction was performed to remove the differences in the color and tone of the images along the edges of any two adjacent tiles. To accomplish this, one tile having a balanced color and tone was chosen as a reference.

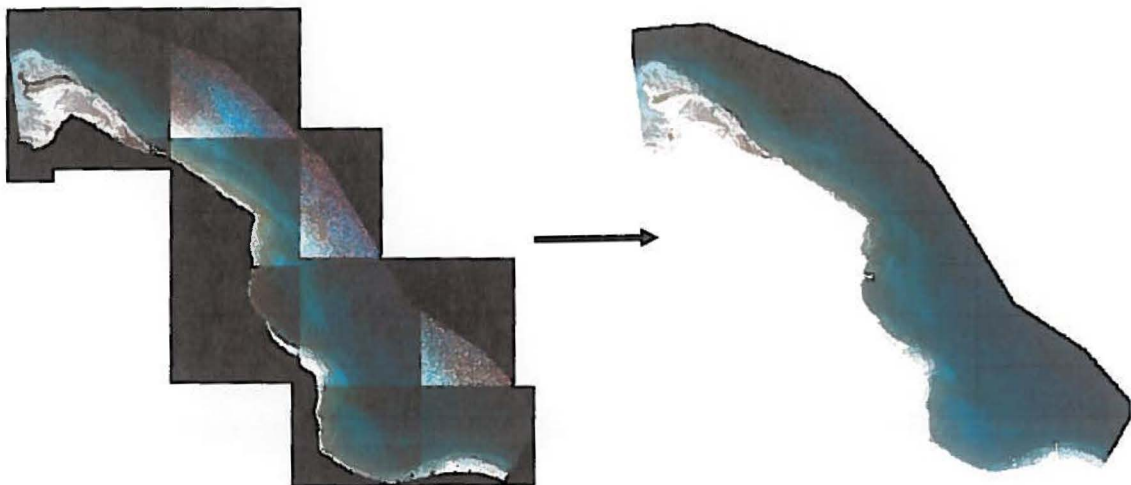


Figure 10 : Twelve tiles of atmospherically corrected image (at the left) assembled in a single composite image (at the right) after applying seamless mosaic

### 3.3.1.4 Resampling

After removing the effect of the atmospheric components, the image was resampled to reduce its size and allow further processing. This was done by applying the Resize feature in ENVI 5.1 and multiplying the image dimensions by a scale factor of 0.3. The values of the image pixels were recalculated using nearest neighbor resampling.

### 3.3.1.5 Water Column Correction

In order to remove light scattering and absorption effects within the water body, Lyzenga method was applied on the atmospherically corrected images resulting in a depth-invariant index (DII) calculated and assigned for every pixel.

The DII method is a 3-steps procedure [21][23].

#### **First step: Linearization of the depth/ radiance relationship**

Radiance attenuates exponentially with depth. It is possible to linearize the dependence of radiance on depth using a natural logarithmic transformation for the chosen pair of bands (Figure 11):

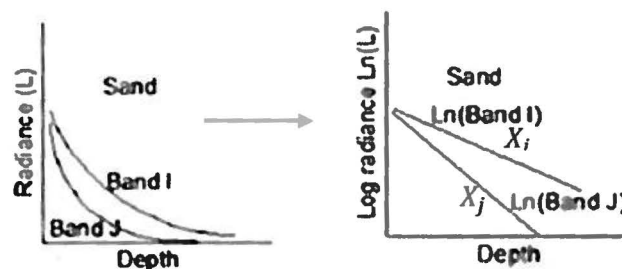


Figure 11 : Graphical representation of the linearization of the depth/radiance relationship for a homogenous bottom type: Sand [24] [17]

$$X_i = \ln(L_i) \quad \text{and} \quad X_j = \ln(L_j) \quad (\text{EQ 2}) (\text{EQ 3})$$

Where,

$L_i$  and  $L_j$  are the pixel radiance for bands  $i$  and  $j$  respectively

$X_i$  and  $X_j$  are the transformed radiance for bands  $i$  and  $j$  respectively

**Second step: Calculation of the attenuation coefficient between pairs of bands**

Bi-plots are created for each pair of spectral bands ( $X_i$  is plotted against  $X_j$ ). The slope of the regression line represents the attenuation coefficient for those bands (Figure 12) and is calculated using equations from previous research [17].

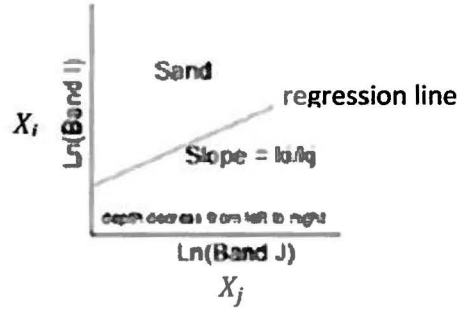


Figure 12 : The regression line of the bi-plot ( $X_i$  against  $X_j$ ) for a homogenous bottom type: Sand. The slope of the regression line represents the attenuation coefficient between the pair of bands  $i$  and  $j$  [24] [17]

$$\frac{k_i}{k_j} = a + \sqrt{a^2 + 1} \quad (\text{EQ 4})$$

Where,

$\frac{k_i}{k_j}$  is the attenuation coefficient between pairs of bands  $i$  and  $j$ ,

$$a = \frac{\sigma_i - \sigma_j}{2\sigma_{ij}} \quad (\text{EQ 5})$$

Where  $\sigma_i$  and  $\sigma_j$  are the variances of bands  $i$  and  $j$  respectively and  $\sigma_{ij}$  is the covariance of both bands  $i$  and  $j$  [26]

$$\sigma_{ij} = \overline{X_i X_j} - (\overline{X_i} \cdot \overline{X_j}) \quad (\text{EQ 6})$$

**Third step: Generation of the depth-invariant index for a homogenous bottom type.**

By plotting  $X_i$  against  $X_j$ , the index of a homogenous bottom type relating to two bands is represented by the intersection value with the  $y$  – axis.

If different bottom types are considered the result of the third step will be represented by two parallel lines with different  $y$  – intercepts (Figure 13).

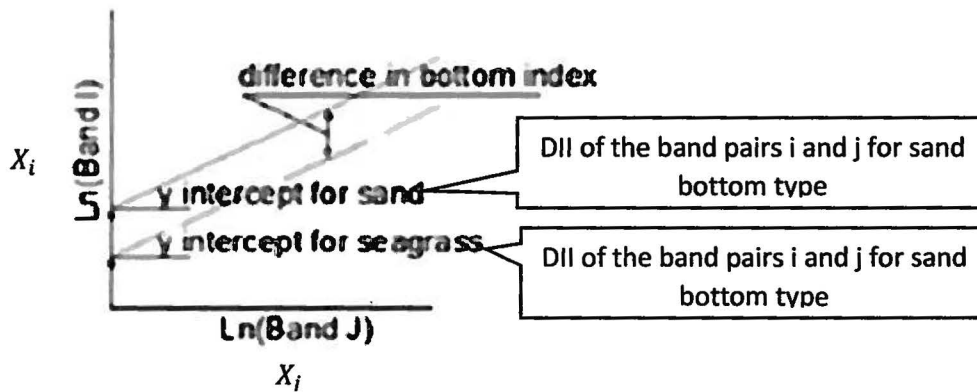


Figure 13 : Different bottom types have the same attenuation coefficient (slope of the regression line) but a different depth invariant index ( $y$  – intercept of the regression line) for the same pair of bands  $i$  and  $j$  [24] [17]

Each pair of spectral band delivers a single DII using the equation:

$$\text{depth invariant index} = X_i - \left[ \left( \frac{k_i}{k_j} \right) X_j \right] \quad (\text{EQ 6})$$

In a previous research Lyzenga's equation which is originally written in radiance was written in terms of reflectance [27]. This has the advantage of obtaining values of atmospherically corrected data.

$$\text{depth invariant index} = \ln(R_i) - \left[ \left( \frac{k_i}{k_j} \right) \ln(R_j) \right] \quad (\text{EQ 7})$$

This is equivalent to calculating  $X_i$  and  $X_j$  in the first step as following:

$$X_i = \ln(R_i) \quad \text{and} \quad X_j = \ln(R_j) \quad (\text{EQ 8}) (\text{EQ 9})$$

Where  $R_i$  represents the pixel reflection for band  $i$ , and  $R_j$  represents the pixel reflection for band  $j$ .

To implement Lyzenga's model on the resampled image and produce index images, a script was written using Interactive Data Language (IDL) (Annex A).

The following steps were considered:

- 1) Eight spectral subsets were generated from the resampled image resulting in 8 images, each displaying one single band.
- 2) Spectral subsets were exported to IDL and assigned to new IDL variables.
- 3) Two spectral subsets were used as parameters with every run of the algorithms.
- 4) All the combination of 2 bands were used resulting in a number of  $P_2^8 - 8$  (48) depth-invariant images.

#### 3.3.1.6 Image Filtering

Bit error filters (an algorithm in ENVI 5.1) was applied on the depth-invariant-index images to suppress the noise that gives the image a salt-and-pepper appearance. Bit Error removal maintains image sharpness and detail while removing noise.

#### 3.3.2 Image processing

Field investigations and video transects revealed four benthic cover types:

- Seagrass: includes Seagrass meadows and Seaweeds characterized by a green color
- Coral: includes live coral
- Macroalgae: includes Macroalgae bed, the most encountered Macroalgae are brown
- Sand: soft bottom dominated by sand

These cover types were selected to extract training data for image processing. A supervised classification procedure was applied and subsequently, an accuracy assessment of the classification results was achieved by calculating confusion matrix using the validation ground truth data.

### 3.3.2.1 Supervised Classification

IDL pre-defined Color table was used to display the depth invariant index image in pseudocolor scale instead of grey luminance scale, in order to increase the level of discrimination of different classes within the image. As a result, 4 out of the 48 preprocessed images were selected to undergo supervised classification because they showed distinguishable classes based on visual interpretation. The 4 selected images differ in the bands of the pair of spectral subsets used while applying the water column correction algorithm: Red edge-Blue, Green – Yellow, Green – Infrared2 and Blue-Green.

Supervised classification algorithm needs to be fed by statistics generated for regions of interests that represent known benthic cover classes. Regions of interests were represented by polygons. Polygons were drawn to cover a group of neighboring pixels that appear fairly homogeneous on the image (determined by similarity in tone and color) and was assigned to one of the pre-defined classes, if a polygon covers more than one coverage type, it was attributed with the dominant one. The choice of the belonging class and the location of the polygon was aided by photointerpretation of the GIS layer that represents the training data. MLC was then applied to perform class assignments based on the pixel Index values of the classification units.

MLC calculates mean values, variance and covariance of the classes providing the probability function). Statistical probability is calculated for a given pixel using mean vectors and variance-covariance values (probability density functions). This is then used to classify an unknown pixel by calculating for each class, the probability that it lies in that class. The pixel is then assigned to the most likely class or if its probability value

fails to reach any close defined threshold in any of the classes, it will be labelled as unclassified [22][28] (Figure 14). MLC algorithm produced a new pseudocolor image where each class is assigned a color.

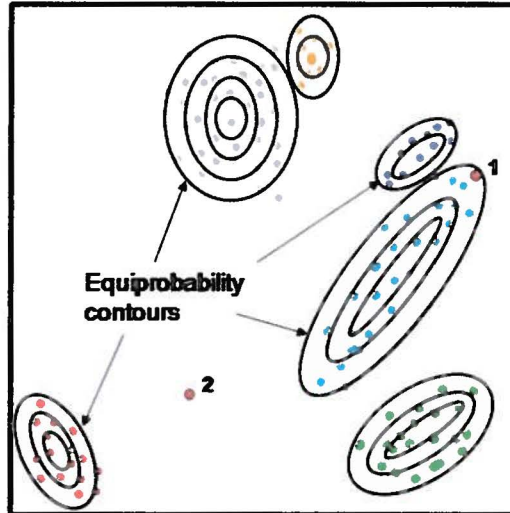


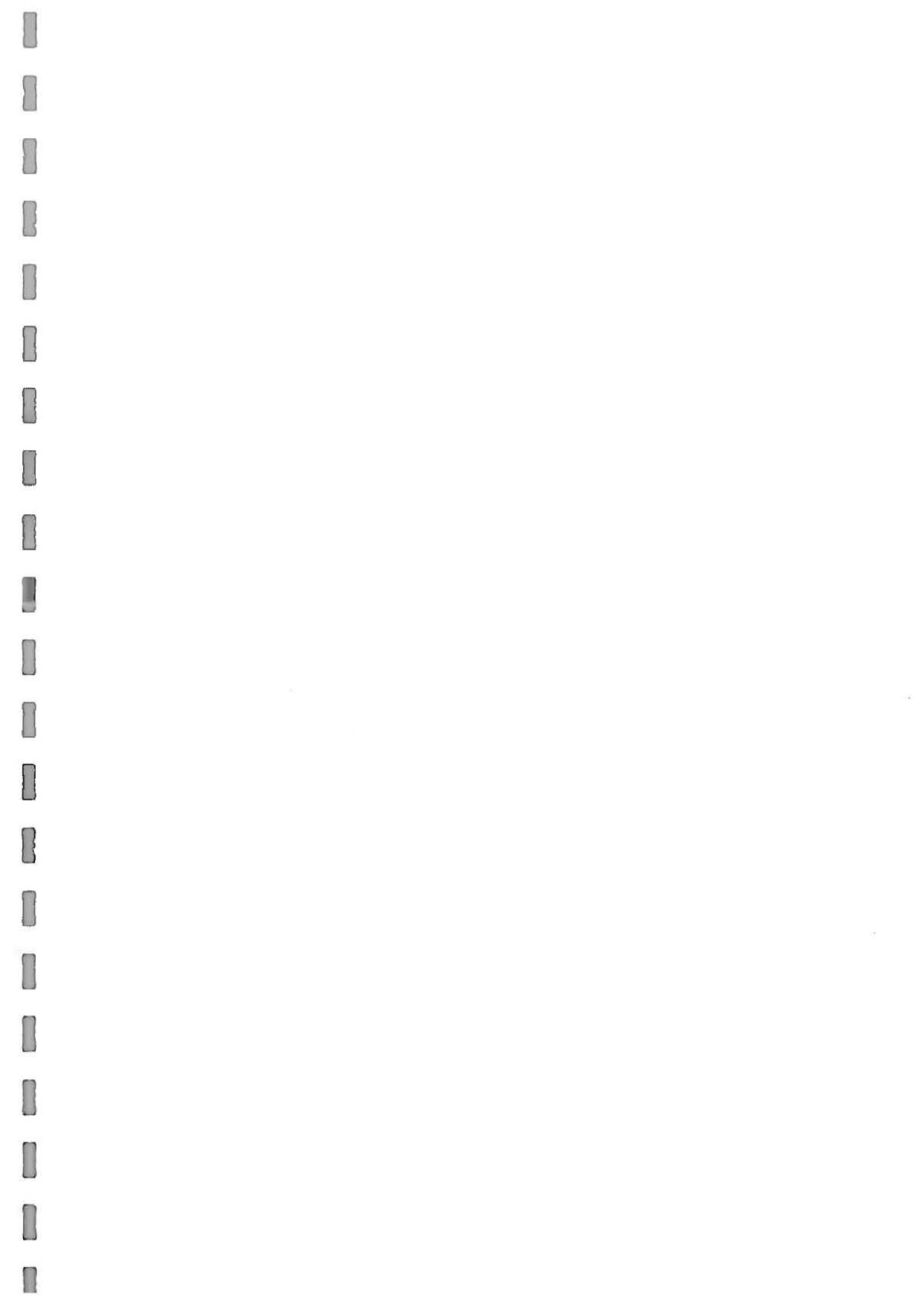
Figure 14 : Schematic representation of pixels classified using Maximum Likelihood Classification [19]

### 3.3.2.2 Validation and Accuracy Assessment

Ground truth pixels were grouped into 4 different categories based on the data recorded by the field survey. These categories are:

- ROI coral
- ROI Seagrass
- ROI Algae
- ROI sand

As described in paragraph 3.3.2.1, MLC algorithm assigned one of the 4 pre-defined benthic classes (Seagrass, Coral, Algae and Sand) to every pixel in the image, hence each ground-truth pixel was also assigned a class.



Assessing the accuracy of the classification is based on calculating ratios and probabilities that reflect how much the categories of the ground-truth pixels are matching with the classes assigned to these pixels. A ground-truth pixel is correctly classified when its category and its class are the same. The classification is considered 100% accurate if all the ground pixels are correctly classified. ENVI 5.1 has a feature that generates two types of confusion matrix (or error matrix), three types of accuracy, two types of errors

1) Ground-truth matrix (pixel): Each column represents the category of the ground-truth pixel (ROI Seagrass, ROI Algae, ROI coral, ROI sand), and every row represents a pre-defined class (Seagrass, Algae, coral and sand). The value  $P_{ij}$  of the element positioned in the  $i^{\text{th}}$  row and  $j^{\text{th}}$  column represents the number of ground-truth pixels belonging to category ( $j$ ) and attributed to class ( $i$ ).  $N$  is the number of classes (4 for the current classification) and  $n$  represents the number of ground-truth pixels (22 for this project)

2) Ground-truth matrix (percent): It shows for every ground-truth category, the percentage of pixels assigned to each of the 4 pre-defined classes.

3) Overall accuracy: It represents the percentage of correctly classified pixels:

$$\text{Overall accuracy} = \frac{\sum_{k=1}^N P_{kk}}{n}$$

2) User accuracy for a class  $i$ : It determines the accuracy of classification for a benthic class  $i$ :

$$\text{User accuracy for class } i = \frac{P_{ii}}{\sum_{j=1}^N P_{ij}}$$

3) Producer accuracy for a category  $j$ : It represents the probability that any pixel belonging to a category  $j$  has been correctly classified:

$$\text{Producer accuracy for category } j = \frac{P_{jj}}{\sum_{i=1}^N P_{ij}}$$

4) Commission error for a class  $i$ : It occurs when the classifier assigns class  $i$  to a ground-truth pixel belonging to a category different than  $i$ :

$$\text{Commission error for class } i = 1 - \frac{P_{ii}}{\sum_{j=1}^N P_{ij}}$$

5) Omission error for a class  $j$ : It occurs when the classification excludes from class  $j$  a ground-truth pixel belonging to category  $j$ :

$$\text{Omission error for class } j = 1 - \frac{P_{jj}}{\sum_{i=1}^N P_{ij}}$$

## Chapter 4

### IMPLEMENTATION AND RESULTS

#### 4.1 Water column correction

Figure 15 shows 4 results of depth- invariant-index images, each generated from a different band ratio (Blue – Green , Red edge – Blue, Green – Infra red2 , Green – Yellow).

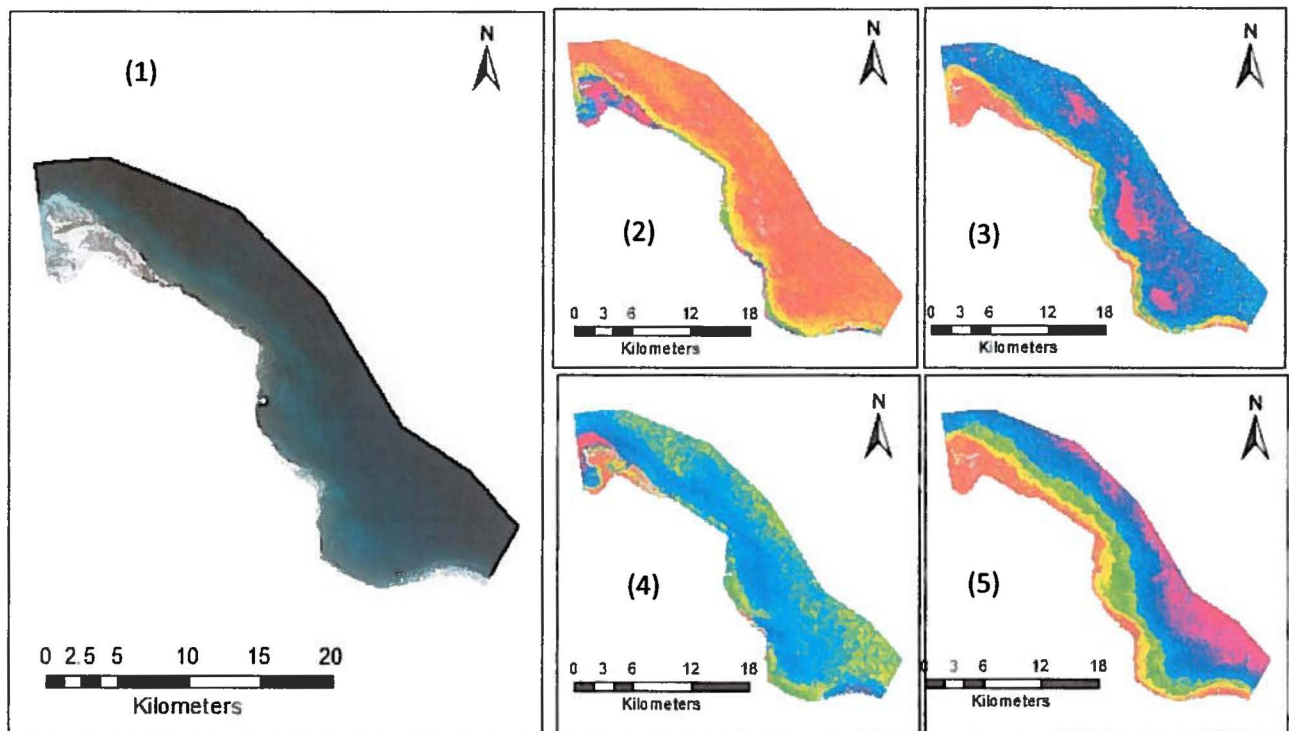


Figure 15 : Atmospherically corrected image in RGB (1), results of the final depth invariant index image for one band ratio: Red edge - Blue (2), Green-Yellow (3), Green-Infra red2 (4), Blue-Green (5)

#### 4.2 Supervised Classification

Maximum Likelihood classification was applied on four pre-processed images that differentiate in the band ratio used for the water column correction (as explained in chapter 3.3.2.1) using 22 training data for four main classes: Algae, Seagrass, Coral and Sand. The resulting classified images are displayed in Figure 16.

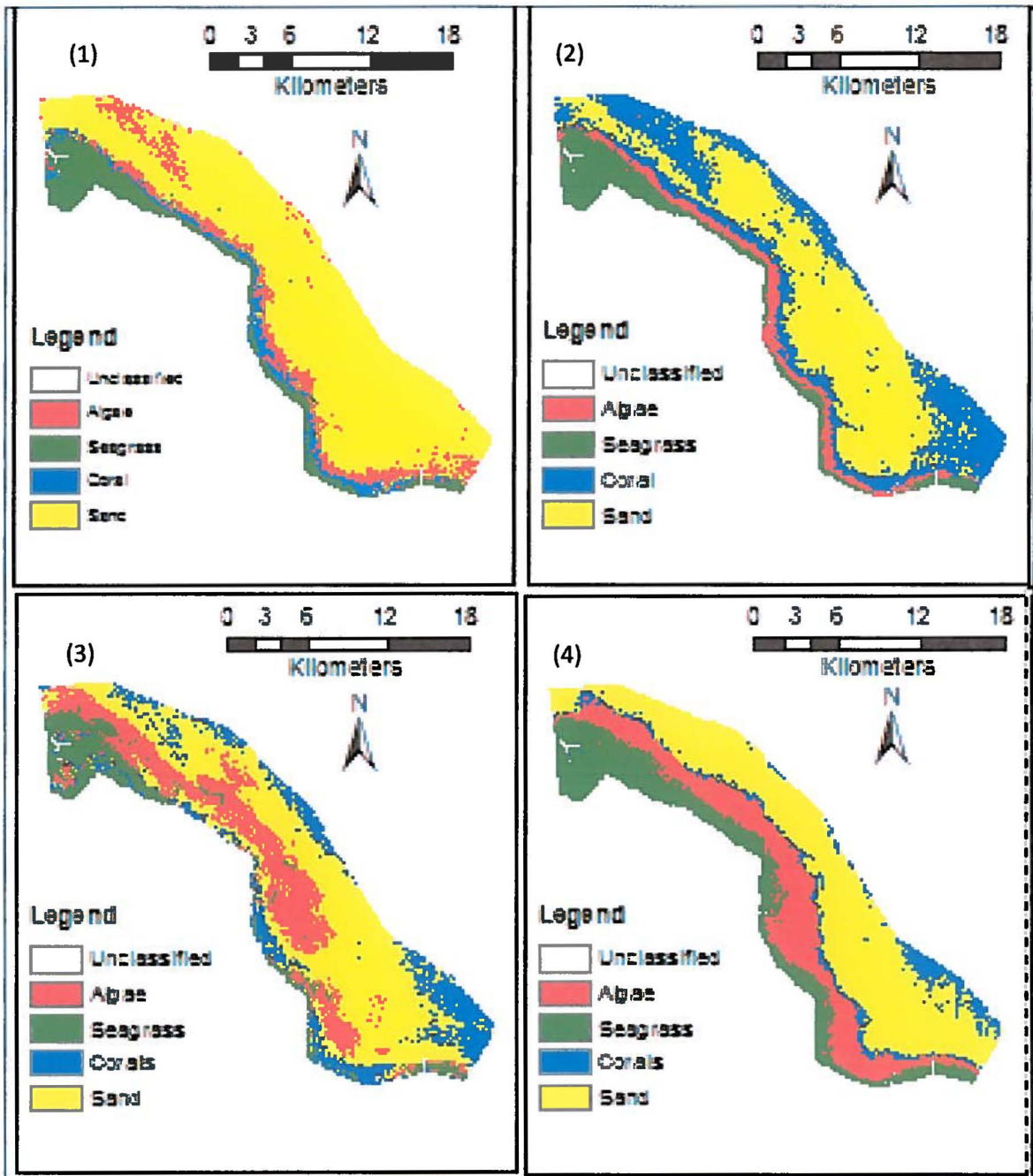


Figure 16 : Classification Results of MLC applied on 4 pre-processed images with different band ratios: Red edge - Blue (1), Green-yellow (2), Green-Infra red2 (3), Blue-Green (4)

Close-ups of these classifications are included in Annex B for a better visualization.

### 4.3 Accuracy Assessment

The accuracy of the 4 classification results was assessed using the same set of 22 ground-truth data pixels. The classification results show that processing the depth

invariant image with band ratio (Green – Yellow) reflects to a large degree actual benthic cover. Whereas the depth invariant images with band ratios (Red edge – Blue, Green-Infra red2 and Blue-Green) show low overall accuracy (Table 3). Producer and user accuracies and errors of commission and omission for the processed image with band ratio (green-yellow) were computed (Table 4).

Table 3 : Overall accuracy of the classification results after processing 4 index images

Band pair	Overall Accuracy
Green – Yellow	81.8%
Red edge – Blue	63.64%
Green – Infra red2	45.45%
Blue – Green	40.91%

Table 4 : Confusion matrix calculated for the classification results of the index image with band ratio (green-yellow)

Class	ROI Algae	ROI Seagrass	ROI Coral	ROI Sand	Total
Algae	5	0	0	0	5
Seagrass	0	0	0	0	0
Coral	1	1	1	0	3
Sand	1	0	1	12	14
Total	7	1	2	12	22

Table 5 : Producer and user accuracies and errors of commission and omission calculated for the classification results of the index image with band ratio (Green-Yellow)

Class	Commission (%)	Omission (%)	Producer Accuracy (%)	User Accuracy (%)
Algae	0	28.57	71.43	100
Seagrass	0	100	0	0
Coral	66.67	50	50	33.33
Sand	14.29	0	100	85.71

## **Chapter 5**

### **DISCUSSION AND LIMITATION**

#### **5.1 Water Column Correction algorithm**

Depth invariant index method was applied to reduce the effect of the water column and generate index images. Other water column correction techniques, such as Bierwirth model, could be used to generate reflectance image, which would allow to benefit from spectral libraries (libraries of spectral signatures containing lists of benthic habitats and their reflectance). However, the lack of spectral measurements of the benthic features and the lack of data about the depth value of every pixel made the choice of water column correction methodology very limited. The classification of the index images produced 4 a-priori broad benthic types (Algae, Seagrass, Coral and Sand). The visual interpretation of index images showed that some band pairs have high potential to discriminate different benthic types (Red edge-Blue, Green-Infra red2, Blue-Green, Green-Yellow), therefore index images with these bands were selected for further classification (Figure 16).

#### **5.2 Field data**

Out of 44 station data, a set of 22 station data was used as training data for Maximum Likelihood classification and the remaining 22 station data was incorporated for accuracy assessment. More reference points dispersed along the entire area of study, at all depths and for all types of cover could improve the classification results and allow more accuracy assessment.

### 5.3 Classification and accuracy assessment

After applying MLC on 4 selected index images, it was noticed that the band pair that has achieved the highest accuracy was Green-Yellow, with an overall accuracy of 81.8% (Table 3). More ground truth data could have produced a better accuracy assessment which will be helpful in future research.

The band pair (green-yellow) was found to be the most appropriate to discriminate between different benthic cover types. This conclusion helps validate the research done by (Loomis, 2009) and (Lee et al, 2011) [32][33].

The user and producer accuracies were high for Algae and Sand, whereas for coral classification the user accuracy was low (33.33%) and the producer accuracy was fair (50%) (Table 5), this is probably due to two main reasons:

- When corals bleach or become stressed they lose their pigmentation and they change their spectral profile which makes them confused with sand cover.
- Some live coral species have spectral signatures similar to that of Seagrass or Algae [29][30][31].

The confusion matrix (Table 4) shows that there is only one ground-truth point belonging to Seagrass category. However, the point had been allocated to coral class creating a confusion which might be probably due to the similarity of the spectral signature of some live coral species and Seagrass. The user and producer accuracies for Seagrass are not reliable due to insufficient ground truth data for Seagrass category.



The classification of bottom type can never be 100% accurate due to the fact that different types of benthic cover can overlap, creating confusion in benthic cover classification.

This project has produced a benthic habitat cover map for the North-Eastern part of the Qatari coastal zone. This map can be used as a stand-alone product to yield useful baseline information to the government, stakeholders and researchers.

## **Chapter 6**

### **CONCLUSION**

In this project, high resolution Worldview-2 data corrected for atmospheric and water column effects was used for extracting benthic cover types in the North-Eastern part of Qatar. 'Depth-invariant bottom indices' were calculated and formed the basis for classification. Training data and ground-truth data from field survey were incorporated to implement the supervised classification and the accuracy assessment. The band pair (Green-Yellow) was found to be the most appropriate band-pair in WV2 to discriminate between the different types of benthic habitats. This conclusion helps validate the researches done by (Loomis, 2009) and (Lee et al, 2011) [32][33].

Processing High resolution satellite imagery supported with field data can be used to classify and map the benthic cover of the coastal marine zone, which can generate valuable information of accessible and inaccessible areas for environmental monitoring, planning and for scientific studies.

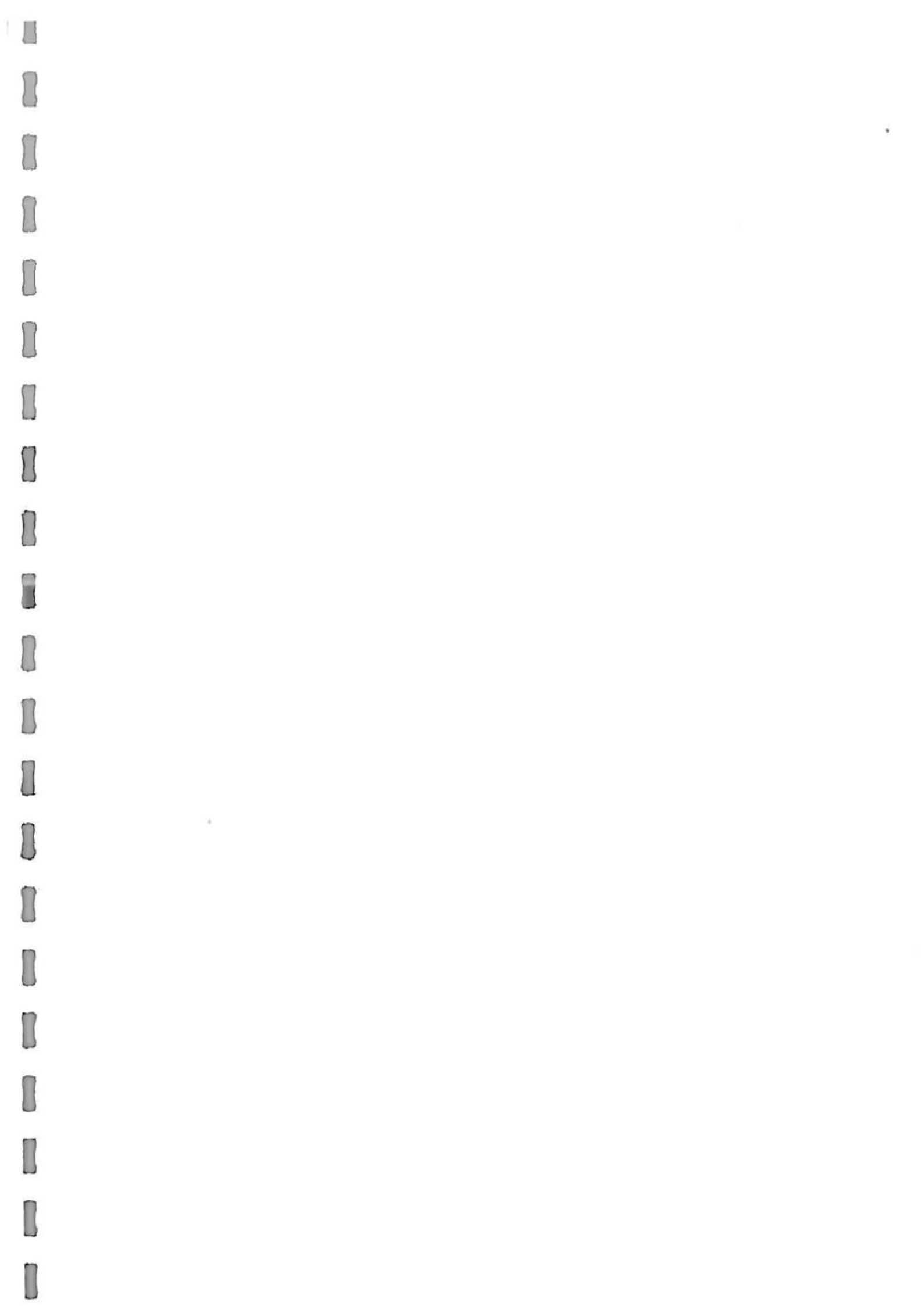
The approach adopted in this project: integration of remote sensing, GIS, and in-situ measurement in studying benthic cover has not been adopted in Qatar before. Therefore, this project will generate interests in the development of future research in this field and within the scientific community. There are several interesting research ideas for future work such as detecting the changes in the benthic cover over time. Further development of the water column correction method can be done incorporating additional amount of field data to study larger areas and extract more features of benthic cover with a higher level of accuracy.

## LIST OF REFERENCES

- [1] General Secretariat For Development Planning, Qatar national vision 2030, 2009. Advancing sustainable development, Qatar's second human development report.
- [2] Nieto P., 2013. Classifying benthic habitats and deriving bathymetry at the Caribbean Netherlands using multispectral Imagery, 1-98 pp
- [3] Arce J.A., 2005. Remote Sensing of Benthic Habitats in southwestern Puerto Rico, University of Puerto Rico Mayaguez Campus.
- [4] Natural resources CANADA, 2014. Website: <http://Canada.gc.ca>
- [5] DigitalGlobe, 2010. White Paper - The benefits of the 8 spectral bands of WorldView-2. Website: <http://www.digitalglobe.com>
- [6] Jensen J. R., 1994. Introductory digital image processing : A remote sensing perspective, 3rd Ed., Prentice Hall. 526 pp.
- [7] Updike T. et al., 2010. Radiometric Use of WorldView-2 imagery, Technical note. DigitalGlobe Inc.
- [8] Edwards A. J., 1999. Radiometric correction of satellite images: When and why radiometric correction is necessary. Applications of satellite and airborne image data to coastal management: Seventh Computer-based Learning Module. Lesson 3, 79 - 102 pp.
- [9] Exelis Visual Information Solutions, 2014. Website: <http://www.exelisvis.com/docs/RadiometricCalibration.html>
- [10] Gurol S. et al., 2008. Tuz Gölü: New absolute radiometric calibration test site. The international archives of the photogrammetry, remote sensing and spatial information sciences, V 37, part B1.

- [11] Elsharkawy A. et al., 2012. Quality control on the radiometric calibration of the WorldView-2 Data, Proceedings of global Geospatial conference.
- [12] Martin J. et al., 2012. Atmospheric correction models for high resolution WorldView-2 multispectral imagery: a case study in Canary Islands, Spain, Remote sensing of clouds and the atmosphere XVII; and Lidar technologies, techniques, and measurements for atmospheric remote sensing VIII. 10 pages.
- [13] Hadjimitsis D. et al, 2009. The use of selected pseudo-invariant targets for the application of atmospheric correction in multi-temporal studies using satellite remotely sensed imagery. International journal of applied earth observation and Geoinformation. Vol 11, 192-200 pp.
- [14] Smith G. M., Milton E. J., 1999. The use of the empirical line method to calibrate remotely sensed data. International Journal of Remote Sensing. Vol. 20, 2635-2662 pp.
- [15] San B.T. et al., 2010. Evaluation of different atmospheric correction algorithms for EO-1 Hyperion Imagery. International Archives of the Photogrammetry. Remote sensing and spatial information Science. Vol. 38 (8).
- [16] Purkis S. et al., 2003. Integrating in situ reef-top reflectance spectra with Landsat TM imagery to aid shallow-tropical benthic habitat mapping. Coral Reefs. Vol. 23, 5–20 pp.
- [17] Green E. et al., 2000. Remote sensing handbook for tropical Coastal Management. Coastal management sourcebooks 3. Chapters 4 and 7.
- [18] Ciralo G. et al., 2006. The classification of submerged vegetation using hyperspectral MIVIS data. Annals of Geophysics. Vol. 49 (1).

- [19] Danoesoebroto A., 2010. Land / Image classification – Supervised & unsupervised classification, Graduate Program of Geodesy and Geomatics Engineering.
- [20] Schowengerdt R. A., 1997. Remote sensing models and methods for image processing. 2nd edition. San Diego, CA. Academic press ltd.
- [21] Lyzenga, D. R., 1981. Remote sensing of bottom reflectance and water attenuation parameters in shallow water using aircraft and Landsat data (Bahamas). International Journal of Remote Sensing. Vol. 2, 71-82 pp.
- [22] Sabins F. F., 1977. Remote sensing: Principles and interpretation, WH Freeman & Co., NY.
- [23] Mumby P. J., 1998. Benefits of water column correction and contextual editing for mapping coral reefs. International Journal of Remote Sensing. Vol. 19, 203-210 pp.
- [24] Deidda M., 2012. Pre-processing of high resolution satellite images for sea bottom classification. Italian Journal of Remote Sensing. Vol. 44, 83-95 pp.
- [25] DigitalGlobe, 2013. Core Product Imagery Guide V 1.2
- [26] Nurlidiasari M., 2005. Mapping coral reef habitat with and without column correction using Quickbird Image. International Journal of Remote Sensing and Earth Sciences. Vol. 2.
- [27] Ben Moussa H., 1989, Télédétection des algues macrophytes de l'Archipel de Molène (France) Radiométrie de terrain et application aux données du satellite SPOT, International Journal of Remote Sensing. Vol. 10 (1), 53-69 pp.
- [28] Lillesand T.M. et al., 1994. Remote Sensing and Image Interpretation 3<sup>rd</sup> Ed., John Wiley & Sons Inc., Toronto and New York.







- [29] Kutser T. et al., 2001. Spectral discrimination of coral reef bottom types. In proceeding of: Geoscience and Remote Sensing Symposium, 2001. IGARSS '01. Institute of Electrical and Electronics Engineers, Vol. 6, 3 pages
- [30] Matsunaga T. et al., 2001. Monitoring of coral reefs on Ishigaki Island in Japan using multitemporal remote sensing data. International Society for Optical Engineering (SPIE), 11 pages.
- [31] Mumby P.J. et al., 2002. Mapping marine environments with IKONOS imagery: enhanced spatial resolution can deliver greater thematic accuracy. Remote Sensing of Environment, Vol. 82 (2-3), 248-257 pp
- [32] Loomis M. J., 2009. Depth derivation from the Worldview-2 satellite using hyperspectral imagery, Unpublished M.S. Thesis, Naval Postgraduate School, Monterey, CA. 53 pages
- [33] Lee K. R. et al, 2011. Determination of bottom-type and bathymetry using WorldView-2, SPIE Proceedings. Vol. 8030, Ocean Sensing and Monitoring III, 80300D, 12 pages.

## Annex A: Algorithm written in IDL to generate the depth-invariant index using Lyzenga method

### Step 1 - Linearization of the depth/ radiance relationship

```
FUNCTION Lyzenga_linearization, band_i
  s=SIZE(band_i)
  A=Make_Array(s[1],s[2],/FLOAT)
  A=band_i
  indices = Where(A NE 0, count)
  IF count GT 0 THEN A[indices] = alog(band_i[indices])
  return, A
```

END

### Step 2 - Calculation of the attenuation coefficient between pairs of bands

```
FUNCTION Lyzenga_calculation_Bands, a, b
  vi=variance(a)
  vj=variance(b)
  covij=correlate(a,b,/COVARIANCE)
  result=(vi-vj)/2*covij
  RETURN, result
END
```

```
FUNCTION Lyzenga_attenuation, a
  return, a+sqrt(a^2 + 1)
END
```

### Step 3 - Generation of the depth-invariant index

```
FUNCTION Lyzenga_DII, band_i, band_j
  e = ENVI(/HEADLESS)
  a=Lyzenga_linearization(band_i)
```

$$X_i = \ln(L_i) \quad \text{and} \quad X_j = \ln(L_j)$$

Where,

$L_i$  and  $L_j$  are the pixel reflectance for bands  $i$  and  $j$  respectively

$X_i$  and  $X_j$  are the transformed reflectance for bands  $i$  and  $j$  respectively

$$\frac{k_i}{k_j} = \alpha + \sqrt{\alpha^2 + 1}$$

Where,

$\frac{k_i}{k_j}$  is the attenuation coefficient between pairs of bands  $i$  and  $j$ ,

$$\alpha = \frac{\sigma_i - \sigma_j}{2\sigma_{ij}}$$

Where  $\sigma_i$  and  $\sigma_j$  are the variances of bands  $i$  and  $j$  respectively and

$\sigma_{ij}$  is the covariance of both bands  $i$  and  $j$

```

b=Lyzenge_linearization(band_j)

c=lyzenge_calculation_Bands(band_i, band_j)
k=lyzenge_attenuation(c)

DII_values=(a-(k*b))

s=SIZE(DII_values)
print, s[1],s[2]

; s[1] and s[2] gives the number of columns and the number of rows

array_values=Make_Array(s[1],s[2],/FLOAT)

array_values=DII_values

file = FILEPATH('R3C1_Band2', ROOT_DIR='C:\R3C1_subsets')
raster = e.OpenRaster(file)

newFile='C:\R3C1_subsets\R3C1_DII_Transformed24'
DII_raster_image=ENVIRaster(array_values, INHERITS_FROM=raster, URI=newFile)
DII_raster_image.Save

print, 'New file written to: '
print, DII_raster_image.uri

RETURN, 'Done'

END

```

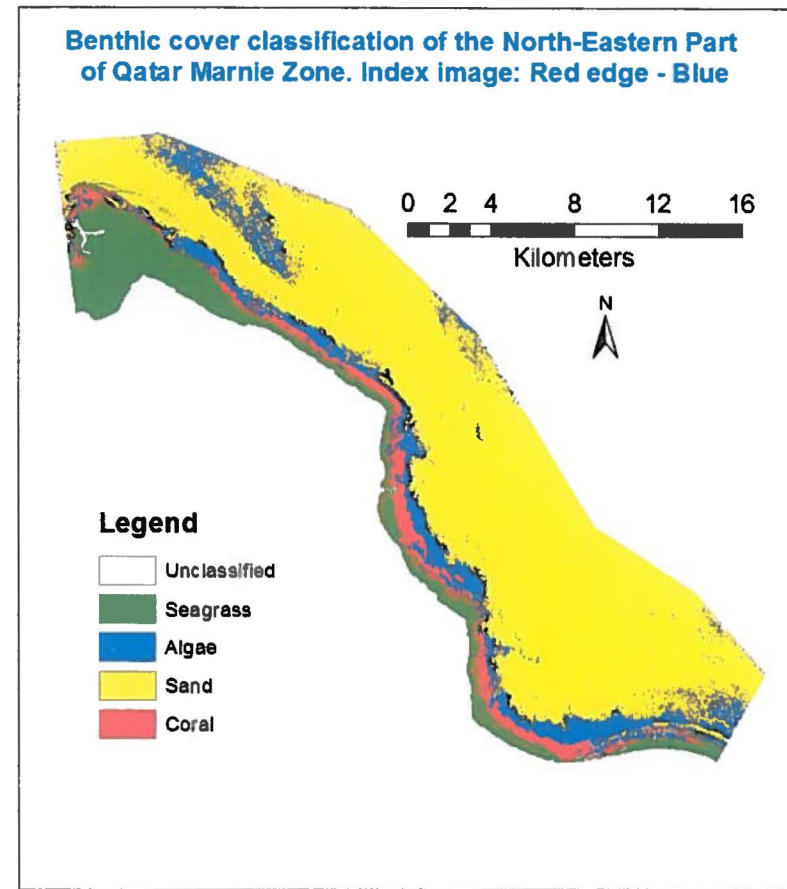
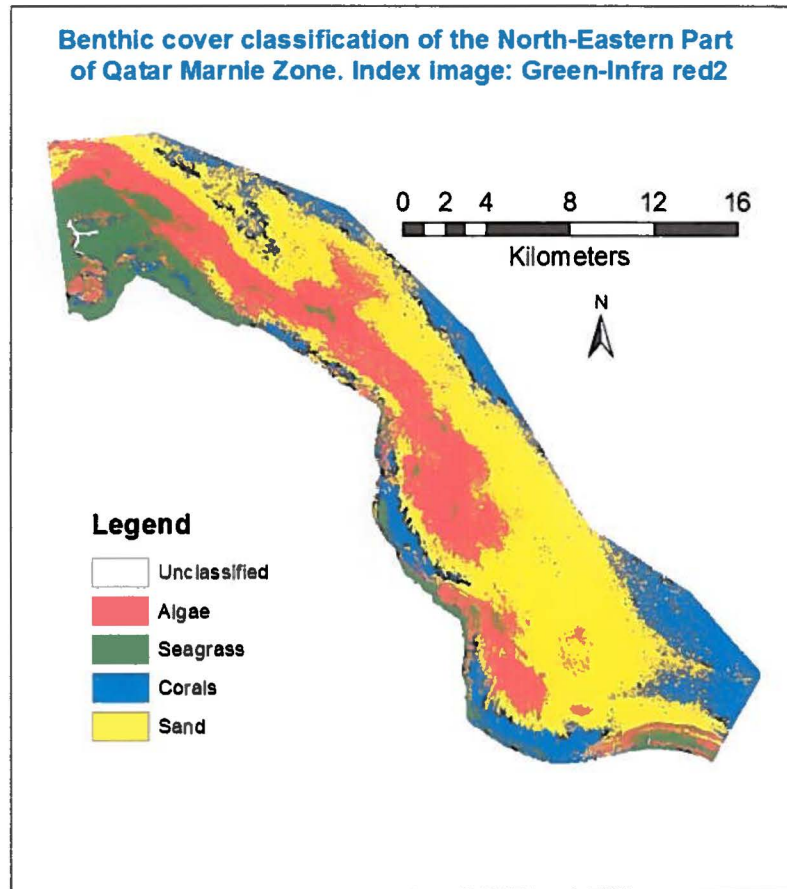
$$\text{depth invariant index} = \ln(R_i) - \left[ \left( \frac{k_i}{k_j} \right) \ln(R_j) \right]$$

$$X_i = \ln(R_i) \quad \text{and} \quad X_j = \ln(R_j)$$

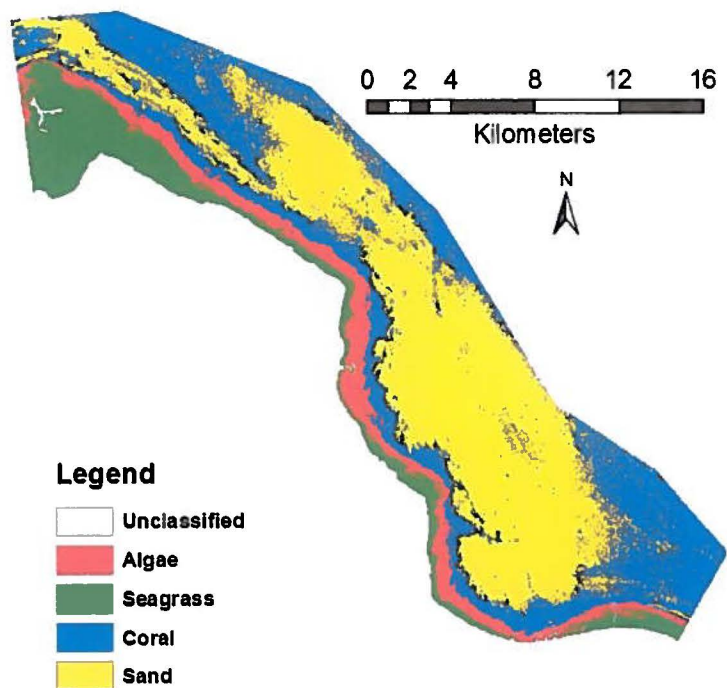
Where  $R_i$  represents the pixel reflection for band  $i$ ,

and  $R_j$  represents the pixel reflection for band  $j$ .

## Annex B : Maps showing benthic cover classification



Benthic cover classification of the North-Eastern Part of Qatar Marnie Zone. Index image: Green-Yellow



Benthic cover classification of the North-Eastern Part of Qatar Marnie Zone. Index image: Blue-Green

